Ultrasonic velocity studies in the vicinity of T_C of bismuth doped manganites

2009 J. Phys.: Condens. Matter 21 056003

(http://iopscience.iop.org/0953-8984/21/5/056003)

J. Phys.: Condens. Matter **21** (2009) 056003 (7pp) doi:10.1088/0953-8984/21/5/056003

Ultrasonic velocity studies in the vicinity of T_C of bismuth doped manganites

G Lalitha and P Venugopal Reddy[1]

Department of Physics, Osmania University, Hyderabad-500007, India

E-mail: paduruvenugopalreddy@gmail.com

Received 28 May 2008, in final form 26 November 2008
Published 12 January 2009
Online at stacks.iop.org/JPhysCM/21/056003

Abstract

Materials with the compositional formula $La_{0.67-x}Bi_xSr_{0.33}MnO_3$ (where $x = 0, 0.1, 0.2, 0.3$) prepared by a citrate gel route were used with a view to investigating the elastic behaviour of manganites in the vicinity of their T_C. The structural characterization of the materials clearly indicates that all the samples have a rhombohedral structure with $R\bar{3}c$ space group. The magnetic (T_C) as well as the metal–insulator (T_P) transition temperatures determined by AC susceptibility and resistivity measurements, respectively, are found to decrease continuously with increasing bismuth concentration. Finally, the ultrasonic longitudinal velocities of all the samples are found to exhibit considerable softening in the vicinity of their magnetic transition temperatures, and an effort has been made to explain the observed behaviour by mean field theory and the Jahn–Teller phenomenon.

1. Introduction

A large change in electrical resistivity in the vicinity of the metal–insulator transition temperature under the influence of a magnetic field is referred to as colossal magnetoresistance (CMR). A large number of rare earth based oxide manganites exhibit a very large negative magnetoresistance of the order of 98%. The correlation between metallic conductivity and ferromagnetism in CMR materials was explained initially by a double exchange mechanism [1]. However, Millis *et al* [2] argued later that the double exchange mechanism alone cannot account for the magnitude of the resistivity drop below T_C. They suggested that the electron–phonon coupling, originally due to Jahn–Teller type distortion around Mn^{3+}, might also play an important role in CMR materials [3].

It is well known that any magnetic transition or changes in magnetic properties are accompanied by transformation or deformation of the crystal lattice [4]. Sound velocity and elastic properties are sensitive to changes in the magnetic state. Apart from this, there is a lot of experimental evidence indicating the presence of electron lattice coupling. For instance, near T_C dramatic changes are observed in the lattice degree of freedom [5], anomalous lattice expansion [6] and anomalous sound velocity hardening, indicating that the lattice is closely related to the electronic and magnetic properties.

[1] Author to whom any correspondence should be addressed.

It was found that the ultrasonic velocities and attenuation of manganites vary anomalously in the vicinity of T_C, indicating that there might be strong electron–phonon coupling in these materials. In fact, the anomalous behaviour of the longitudinal velocity in the vicinity of T_C suggests that the Jahn–Teller effect might be playing an important role in the explanation of the physics behind manganites.

Ceramic oxides are difficult to densify below 1500 °C [7]. For cost effectiveness, preparation of the materials at low sintering temperatures is desirable. Sintering temperatures ranging from 1350 to 1500 °C are used for the preparation of rare earth based CMR materials by a solid state reaction method, depending on dopant concentration, starting materials etc. This may in turn result in considerable crystallite growth leading to poor mechanical properties. In general, in order to overcome the sintering related problems, bismuth oxide is normally used as a sintering aid. In the present investigation, an effort has been made to investigate whether the addition of bismuth oxide influences the elastic behaviour of CMR materials in general and LSMO in particular; the results are presented here.

2. Experimental details

Bulk polycrystalline samples with compositional formula $La_{0.67-x}Bi_xSr_{0.33}MnO_3$ (where $x = 0, 0.1, 0.2, 0.3$) were prepared by the sol–gel process. In this process, high purity

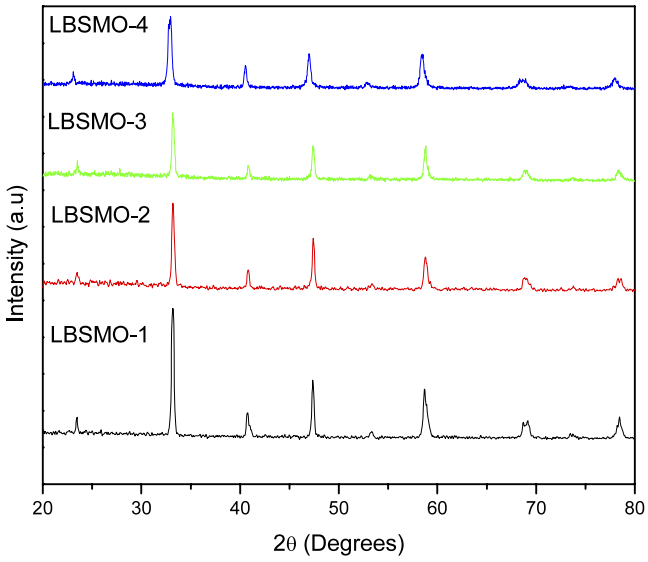

Figure 1. XRD patterns of bismuth doped manganites. (This figure is in colour only in the electronic version)

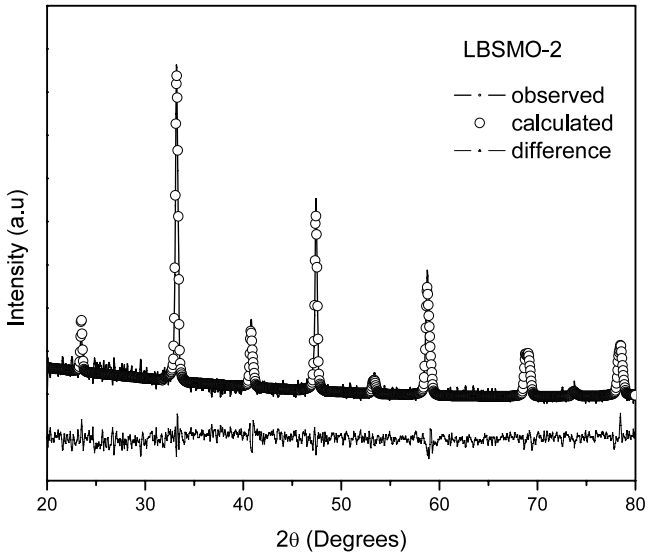

Figure 2. Rietveld profile fit for the x-ray diffraction pattern of $La_{0.57}Bi_{0.1}Sr_{0.33}MnO_3$.

starting materials taken in stoichiometric ratio were converted into nitrates and then into citrates. The pH of the solution is adjusted between 6.5 and 7.0 and the clear solution was allowed to evaporate slowly. A gelating reagent, ethylene glycol, was added and the solution was heated at 200 °C to obtain a gel. On further heating this gave a dry fluffy precursor, which was later calcined at 1000 °C. The powder was pressed into pellets and finally sintered in air at 1200 °C for 4 h.

All the materials were characterized by x-ray diffraction using a Phillips Expert diffractometer with Cu Kα (λ = 1.541 Å) radiation. Scanning electron microscopy (SEM) was performed on (Hitachi model S3700N) to examine the surface morphology of the samples, while the electrical resistivity measurements were carried out over a temperature range of 80–300 K mainly to determine the T_P values. The magnetic transition temperatures (T_C) were also determined by measuring the AC susceptibility (χ) using the mutual inductance bridge principle. The error in the measurement of both these parameters is $\pm 0.5°$.

The bulk densities (ρ) of the samples were measured using the immersion method. In this method, first the weight of the sample in air (D) is measured and then weight of sample in kerosene (I) medium was measured. Later the sample was immersed in kerosene and placed in a vacuum chamber and evacuated so that the pores of the sample were filled with kerosene. Later, the saturated weight of the sample (S) was measured, and using these data the bulk densities of the samples were calculated. The x-ray densities (ρ_0) were calculated from lattice parameters obtained from XRD data and using the bulk and x-ray densities, the porosity values of all the samples were also calculated.

Finally, with a view to investigating the behaviour of ultrasonic velocities, especially in the vicinity of magnetic transition temperature (T_C), the longitudinal velocity measurements were undertaken by the pulse transmission technique in the temperature region 200–400 K using a specially designed sample holder CAASS [8]. This sample holder was designed so that there is no need to use acoustic couplants for the measurements. The percentage of error in the measurements is about 1%.

3. Results and discussions

3.1. General

The x-ray diffraction patterns of all the samples were recorded at room temperature and the plots are shown in figure 1. The crystallographic data obtained from the XRD pattern were refined by Rietveld's profile fitting technique using the FullProf [9] software package and one of the refined XRD patterns is shown in figure 2. After analysing the refined patterns, it has been concluded that all the samples are of single phase with rhombohedral structure and space group $R\bar{3}c$. Further, using the refined patterns the unit cell parameters of all samples were computed and are given in table 1. In the table, R_P is R-pattern, R_{WP} is R-weighted pattern, R_E is R-expected and S is goodness of fit (ratio of R_{WP} and R_{EXP}). It is known that when the S value is $\sim$1, the fitting is expected to be very good. It can be seen from the table that although the cell parameter 'c' increases considerably, there is surprisingly only a slight enhancement of the other parameter 'a'. It is also interesting to note from the table that the Mn–O–Mn bond angle remains constant, while the bond length is increasing with increasing bismuth concentration. The SEM measurements of all the materials were undertaken and are shown in figure 3. It can be seen from the figures that the size and geometrical shape of the pores are found to vary randomly. It is also interesting to note from table 2 that both bulk and x-ray densities are found to increase with increasing bismuth concentration.

Resistivity measurements were undertaken in the temperature range 80–300 K to determine the metal–insulator transition (T_P) temperatures and the plots of resistivity versus

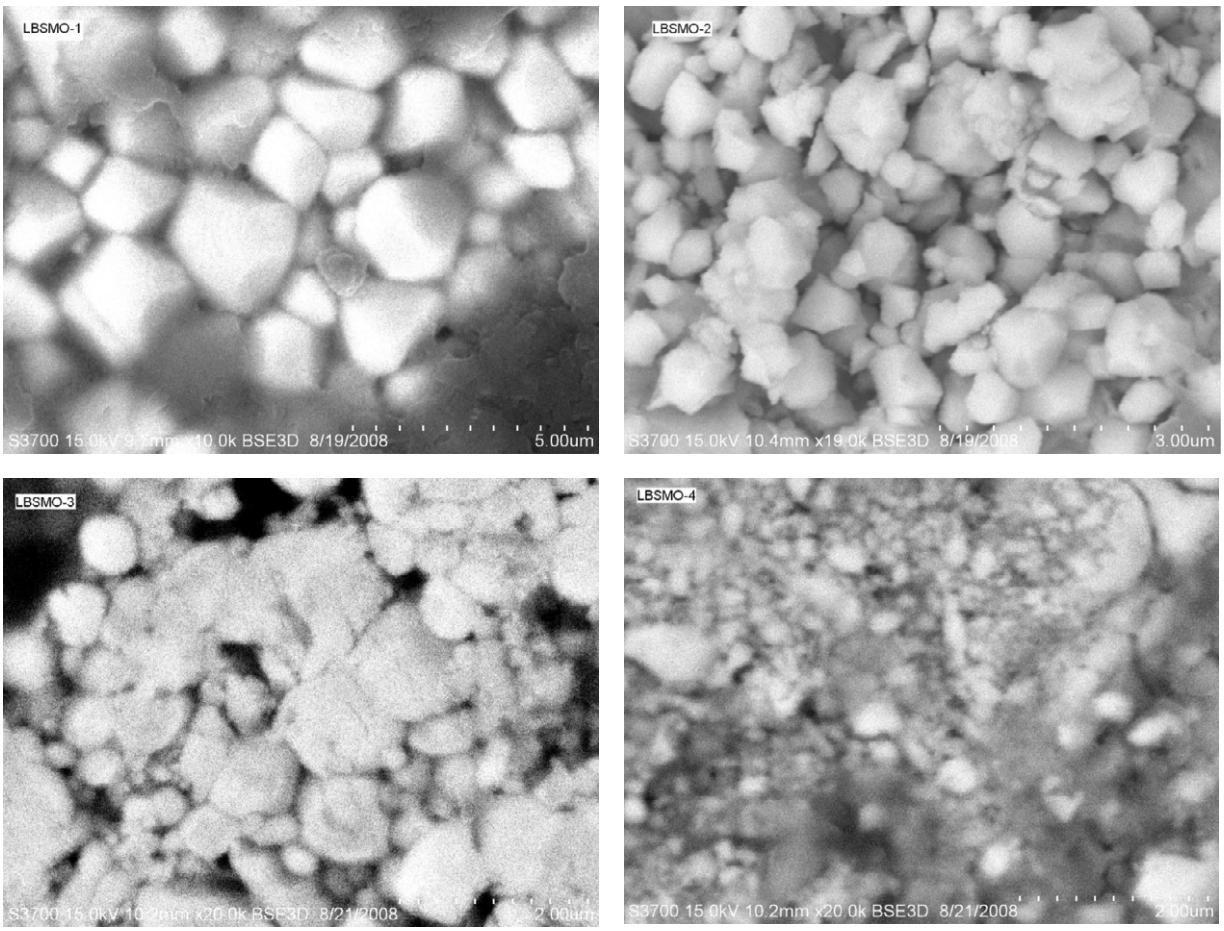

Figure 3. SEM images of $La_{0.67-x}Bi_xSr_{0.33}MnO_3$ (where $x = 0, 0.1, 0.2, 0.3$).

Table 1. Crystallographic data for Bi doped manganites. (Note that the atoms are located at the following Wyckoff positions for the $R\bar{3}c$ space group, La(Bi, Sr) 6(a): (0, 0, 3/4); Mn 6(b): (0, 0, 0); O18(e): (x, x, 1/4).)

Sample	$La_{0.67}Sr_{0.33}MnO_3$	$La_{0.57}Bi_{0.1}Sr_{0.33}MnO_3$	$La_{0.47}Bi_{0.2}Sr_{0.33}MnO_3$	$La_{0.37}Bi_{0.3}Sr_{0.33}MnO_3$
Sample code	LBSMO-1	LBSMO-2	LBSMO-3	LBSMO-4
a(Å) = b (Å)	5.495(3)	5.496(8)	5.500(6)	5.509(3)
c (Å)	13.367(1)	13.377(3)	13.410(3)	13.412(1)
Structure type	Rhombohedral	Rhombohedral	Rhombohedral	Rhombohedral
Space group	$R\bar{3}c$	$R\bar{3}c$	$R\bar{3}c$	$R\bar{3}c$
Mn–O–Mn	176.8	176.8	176.8	176.8
Bond angle (°)				
Mn–O–Mn	1.939	1.940	1.942	1.945
Bond length (Å)				
O(x)	0.49	0.49	0.49	0.49
R_P (%)	7.21	7.18	7.34	6.74
R_{WP} (%)	9.19	8.95	9.47	9.61
R_{EXP} (%)	8.89	8.80	9.07	9.40
Goodness of fit (S)	1.07	1.03	1.09	1.05

Table 2. Transition temperatures and room temperature elastic data.

Sample code	T_C (K)	T_P (K)	Bulk density (kg m^{-3})	X-ray density (kg m^{-3})	Porosity (%)	V_l (m s^{-1})	V_s (m s^{-1})
LBSMO-1	350	296	5649	6477	13	3500	2042
LBSMO-2	322	176	5765	6671	14	3931	2148
LBSMO-3	313	136	5844	6846	15	4160	2251
LBSMO-4	276	90	6113	7022	13	4308	2354

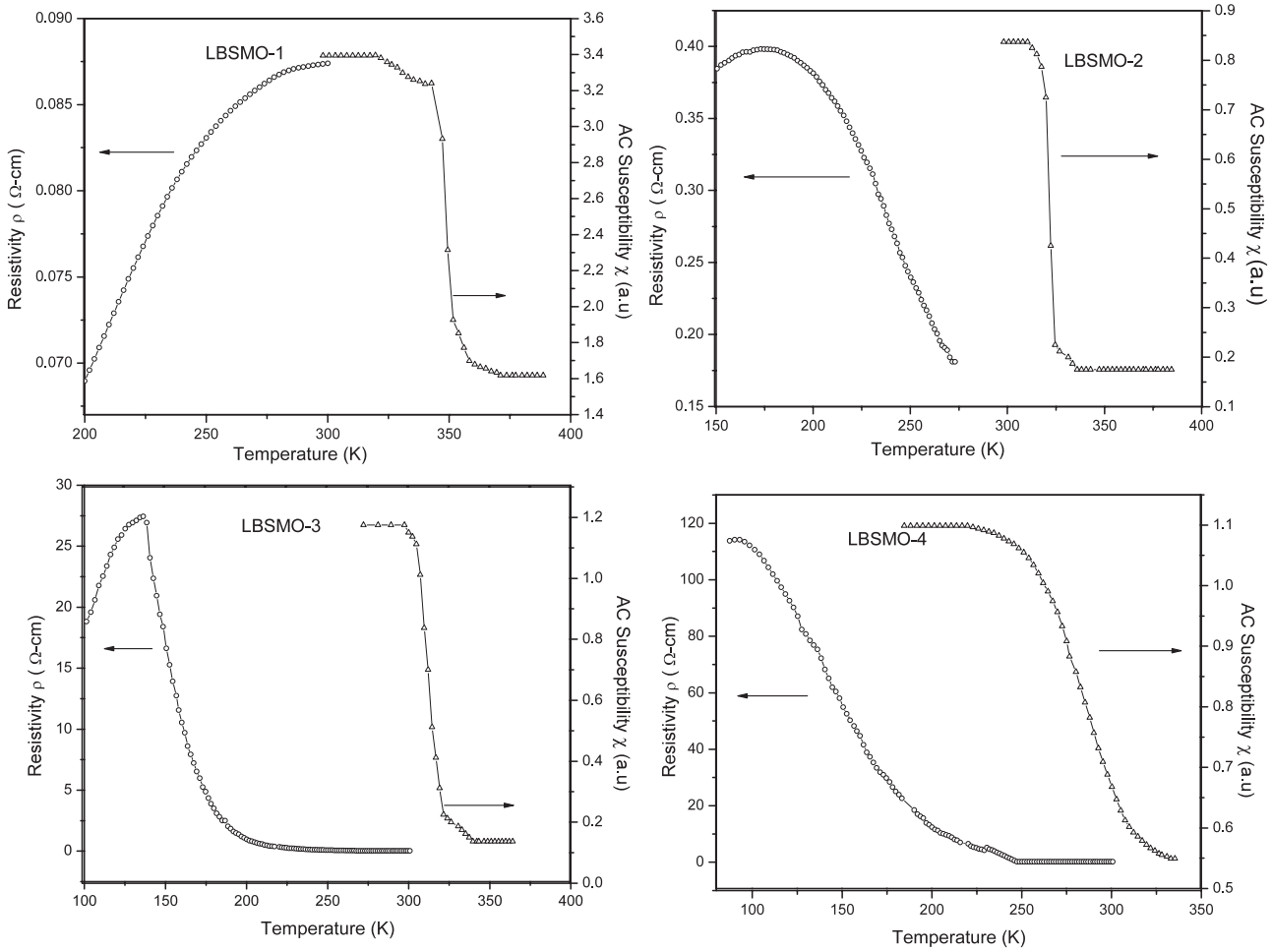

Figure 4. Resistivity and AC susceptibility plots of bismuth doped manganites.

temperature are shown in figure 4. T_P values obtained from the plots are given in table 2 and are found to decrease continuously with increasing bismuth concentration. A systematic investigation of AC susceptibility (χ) with temperature over the temperature range 200–400 K has been undertaken and the corresponding plots are shown in figure 4. Based on these results, the ferro- to paramagnetic transition temperatures (T_C) were obtained from the inflection point of $d\chi/dT$ versus T (K) curves and are also given in table 2.

3.2. Room temperature elastic behaviour

Using X-cut and Y-cut 1 MHz PZT crystals, the longitudinal and shear wave velocities of all the samples were obtained and are given in table 2. The information about the bulk and x-ray densities is essential for calculating the elastic moduli. Therefore, the bulk densities of all the samples were obtained by the immersion method and are also included in table 2. It can be seen from the table that both the velocities are found to increase with increasing bismuth concentration and the observed behaviour is expected due to continuous doping of bismuth.

3.3. Porosity correction

The elastic moduli of solid state materials in general and ceramics in particular depend on their density. As the materials under study are found to be porous, the measured elastic moduli do not have any significance unless they are corrected to zero porosity. The strength of a porous material depends on pore distribution, morphology and size, with high porosity leading to low strength. Further, ceramics inherently have random microstructures with pores having random shape, size and distribution. Even in the case of samples of the present investigation, the shape and size of the pores are irregular (figure 3). Most of the models available in the literature are either empirical or analytical and deal with geometrically regular pore shapes and idealized pore distributions; none of them take account of the pores having random size and shape. However, Wagh *et al* [10] in their model taking random size of the pores into consideration formulated an equation

$$E = E_0(1 - P)^m \tag{1}$$

where P is the porosity, E is elastic modulus of porous material, E_0 is non-porous elastic modulus and m is a constant. This model was applied to a large number of ceramics including Y–Ba–Cu–O superconductors [11, 12]. It was found that the value of m is 2 for most of the standard ceramics unless hot pressing is used during the synthesis processes. Therefore, the elastic moduli of all the materials in the present investigation have been corrected to zero porosity using the

Table 3. Elastic moduli corrected to zero porosity.

Sample	E_0 (GPa)	η_0 (GPa)	σ_0	V_m (m s^{-1})	θ_D (K)
LBSMO-1	77.29	31.18	0.24	4746	475
LBSMO-2	92.62	35.97	0.29	5048	505
LBSMO-3	106.02	40.97	0.29	5320	531
LBSMO-4	115.60	44.92	0.29	5493	548

above equation and the void-free Young's and rigidity moduli are given in table 3.

The acoustic Debye temperature provides useful information about the physical properties of the solids in general and CMR materials in particular. As such, the Debye temperatures of all the materials have been calculated using Anderson's relation [13]

$$\theta_D = h/k[(3qN/4\Pi)(\rho_m/M)]^{1/3}V_m \tag{2}$$

where h is the Planck constant, k is the Boltzmann constant, N is the Avogadro number, M is the molecular weight of the sample, q is the number of molecules in the unit cell and ρ_m is the density of the sample. The average sound velocity V_m has been calculated using the formula [13]

$$V_m = [1/3(2/V_s^3 + 1/V_l^3)]^{-1/3}. \tag{3}$$

The computed values of V_m along with those of Debye temperature (θ_D) are given in table 3. It can seen from the table that both the elastic moduli (E_0 and η_0) along with Debye temperatures are increasing with increasing bismuth concentration, thereby indicating that addition of bismuth is beneficial.

3.4. Variation of elastic behaviour with temperature

To gain an insight into the elastic behaviour of the materials of the present investigation, especially in the vicinity of their T_C, the longitudinal velocities of all the samples have been measured over the temperature range 200–400 K and the corresponding plots are shown in figure 4. It can be seen from the figures that the longitudinal velocity of the samples LBSMO-2, LBSMO-3 and LBSMO-4, after an initial increase, is found to decrease continuously with decreasing temperature, reaching a minimum value at their respective T_Cs. In contrast, the longitudinal velocity of sample LBSMO-1 decreases continuously right from 400 K onwards. However, on further decrease of temperature beyond T_C, the ultrasonic velocities of all the samples are found to increase continuously. As a matter of fact, a close examination of the figures indicates that the ultrasonic velocity would have increased linearly with decreasing temperature but for softening behaviour in the vicinity of their T_C. Therefore, it has been concluded that all the samples in the present investigation exhibit considerable elastic softening in the vicinity of their T_C s. In fact, such a phenomenon is not a new one, as a similar behaviour has been reported in the case of Zn doped La–Ca manganites [14], Y doped La–Ca manganites [15], La–Ca manganites [16], La–Ba manganites and La–Sr manganites [17] etc.

The observed anomalous behaviour, especially in the vicinity of T_C, may be explained using a theoretical model. In recent times, although several theoretical models have been proposed, mean field theory incorporating the ideas relating to the Jahn–Teller effect [18] seems to better explain the anomalous behaviour of magnetic oxides in general and manganites in particular in the vicinity of their magnetic transition temperature T_C. In fact, Chen *et al* [19, 20] explained the anomalous behaviour of elastic moduli of some manganites using mean field theory and the Jahn–Teller theorem by assuming that Jahn–Teller distortion transforms from the dynamic type ($T > T_C$) to the static type ($T < T_C$). Therefore, an attempt has been made to explain the anomalous elastic behaviour in the vicinity of T_C observed in the samples in the present investigation using the mean field theory.

The important criterion on which the theory was developed is the existence of an interaction between a lattice distortion (i.e. elastic strain) and wavefunction of a degenerate ground state, which lifts the degeneracy causing the molecule to seek a distorted configuration of lower energy [21]. Considering the material to be a set of N weakly interacting degenerate two-level systems, whose ground state is degenerate and widely separated from the excited states [22], the Hamiltonian of the system is given by

$$\mathcal{H} = 2c^o e^2 - (\eta e + \lambda\langle\sigma\rangle)\Sigma\sigma(l) \tag{4}$$

where the first term represents the elastic distortion energy, while the second term is the Jahn–Teller interaction between the strain, e, and N two-level systems. η is the interaction constant while $\sigma_Z(l)$ is the Pauli spin operator with eigenvalues ± 1 and c^0 is the elastic restoring force constant. The action of the strain in splitting the degenerate energy levels is the then same as if a magnetic field were applied to lift the magnetic degeneracy of a true spin $= 1/2$ system.

The equilibrium configuration of a crystal at given temperature T is determined by the minimum of thermodynamic free energy and is given by

$$F = \langle\mathcal{H}\rangle - TS \tag{5}$$

where S is the entropy and $\langle\mathcal{H}\rangle$ is the thermal expectation value of the Hamiltonian and is equal to the energy E. Therefore, for N two-level systems we have [21]

$$F = U - kT\ln Z \tag{6}$$

where U is the internal energy and Z is the partition function of the whole system. On substituting the values of U and Z in equation (6), the total free energy is given by

$$F = N\lambda\langle\sigma\rangle^2 + 2c^0e^2 - 2NkT\ln[2\cosh\beta\Delta] + \sum\{1/2h\omega_\alpha(q) + kT\ln(1-\exp[-\beta h\omega_\alpha(q)])\}. \tag{7}$$

Now, the stress is defined as the first derivative of free energy w.r.t strain and is given by

$$X = c^0(e - (\mu/\eta)\langle\sigma\rangle. \tag{8}$$

The isothermal elastic constant is defined as the strain derivative of stress, and on simplifying

$$c^T(T) = c^0\{[1 - (\lambda+\mu)\chi^T(T)]/[1 - \lambda\chi^T(T)]\}. \tag{9}$$

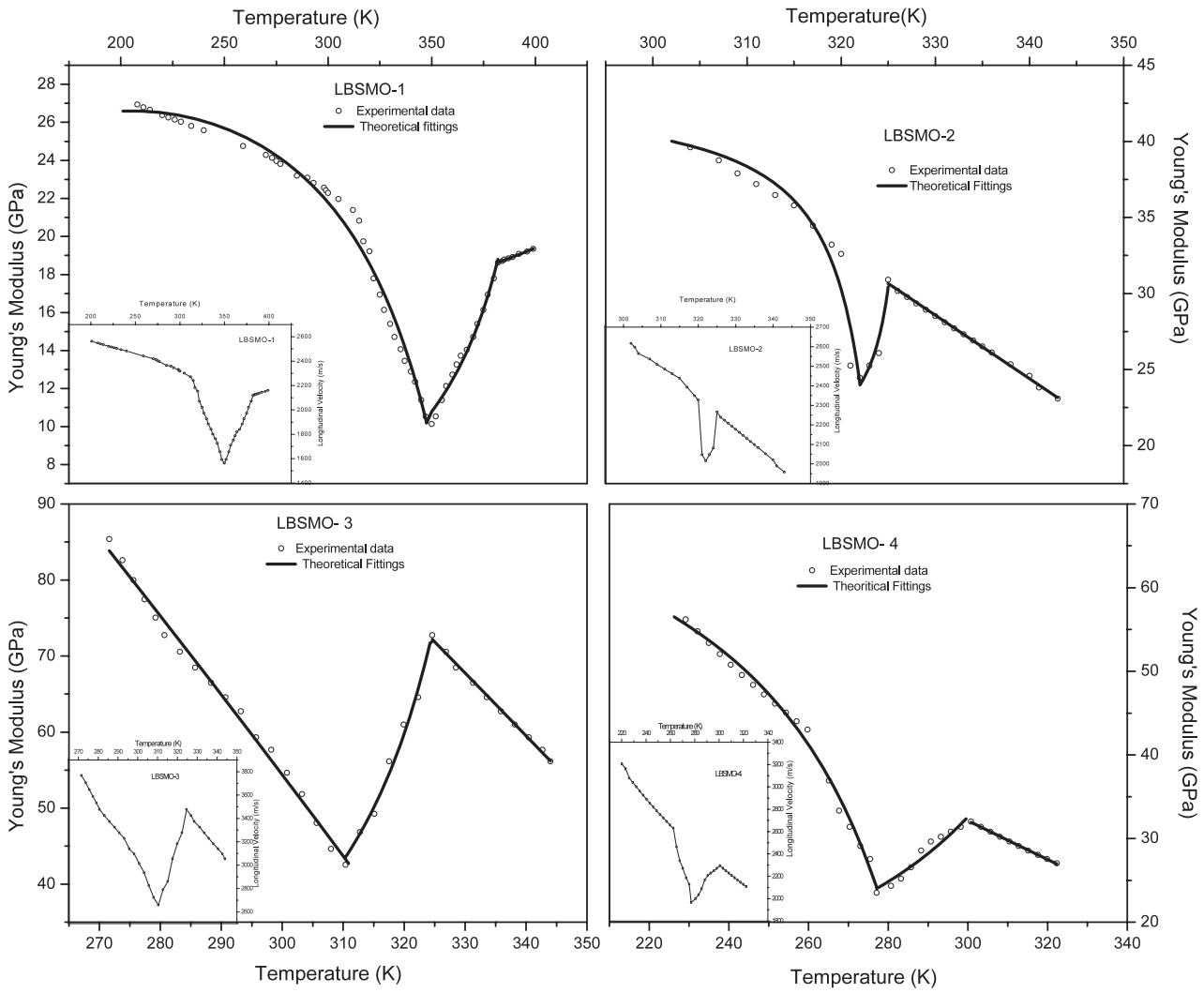

Figure 5. Ultrasonic longitudinal velocities and theoretical fittings of elastic moduli for bismuth doped manganites.

The system exhibits anomalous elastic behaviour at $T = T_C$ only if susceptibility obeys the relation

$$\chi^T(T_C) > 1/(\lambda + \mu). \tag{10}$$

Therefore, for $T < T_C$ the susceptibility value is

$$\chi^T = 1/kT \cosh^2(\Delta/kT) \tag{11}$$

for $T > T_C$, $\Delta \to 0$ and $\chi^T = 1/kT$. On substituting χ^T values in equation (9) we get

$$c^T(T) = c^0\{[T - (\lambda + \mu)/k \cosh^2(\Delta/kT)]/ [T - \lambda/k \cosh^2(\Delta/kT)]\} \quad \text{for } T < T_C \tag{12}$$

$$\text{and } c^T(T) = c^0\{[T - T_C^0)]/[T - \theta]\} \quad \text{for } T > T_C \tag{13}$$

where θ is the phonon exchange constant.

It is interesting to note from equations (12) and (13) that as $T \to T_C$, the elastic restoring force associated with the strain e approaches zero, thereby indicating that the crystal becomes unstable at $T = T_C$ due to distortion associated with the strain e. Therefore, one may conclude that equations (12) and (13) explain the anomalous behaviour of a material at temperatures of both $T < T_C$ and $T > T_C$. For the purposes of computational convenience, the experimentally observed longitudinal velocities have been converted into Young's moduli and are used in the present investigation.

Thus the experimental data for all the samples in the present investigation both below and above T_C were fitted to equations (12) and (13), respectively, and the fittings are shown in figure 5. In the figure, the open circles indicate the experimental data points while the solid lines are theoretical curves. In order to verify the quality of theoretical fittings, the linear regression coefficients (R^2) of all the samples have been calculated and it has been concluded that both the equations match well with the experimental data from the present investigation. The best fit parameters, c^0, Δ, $(\lambda + \mu)/k$, λ/k, T_C^0 and θ obtained for all the samples in the present investigation are given in table 4.

4. Conclusions

(1) The ultrasonic longitudinal velocities of all the Bi doped La–Sr manganites are found to exhibit considerable softening in the vicinity of their magnetic transition temperature, T_C.

Table 4. Best fit parameters for elastic moduli.

Sample	c^0/c_{min}	$(\lambda+\mu)/k$ (from equation (12)) (meV)	λ/k (from equation (12)) (meV)	Δ	c^0/c_{min}	T_C^0 (from equation (13)) (K)	θ (from equation (13)) (K)
LBSMO-1	3.93	41.16	47.21	10.62	4.32	380	424
LBSMO-2	1.71	37.67	37.90	2.21	0.76	329	328
LBSMO-3	1.05	37.09	35.58	2.21	0.78	321	310
LBSMO-4	4.31	33.60	37.09	0.033	2.61	300	297

(2) The anomalous variation of ultrasonic velocity in the vicinity of the magnetic transition temperature may be explained on the basis of mean field theory and the Jahn–Teller phenomenon.

Acknowledgment

One of the authors (G Lalitha) thanks CSIR for providing a SRF fellowship.

References

[1] Zener C 1951 *Phys. Rev.* **82** 403
[2] Millis A J, Shraiman B I and Mueller R 1996 *Phys. Rev. Lett.* **77** 175
[3] Zhu C and Zheng R 1999 *Phys. Rev.* B **59** 11169
[4] Hwang H Y, Cheong S W, Radaelli P G, Marezio M and Batlogg B 1995 *Phys. Rev. Lett.* **75** 914
[5] Belevtsev B I, Zvyagina G A, Zhekov K R, Kolobov I G, Yu Beliayev E, Panfilov A S, Galtsov N N, Prokhvatilov A I and Fink-Finowicki J 2006 *Phys. Rev.* B **74** 054427
[6] Ramirez A P, Schiffer P, Cheong S-W, Chen C H, Bao W, Palstra T T M, Gammel P L, Bishop D J and Zegarski B 1996 *Phys. Rev. Lett.* **76** 3188
[7] Fu Y-P, Tseng C-W and Peng P-C 2008 *J. Eur. Ceram. Soc.* **28** 85
[8] Ramana Y V and Venugopal Reddy P 1989 *Acoust. Lett.* **13** 83
[9] Carvajal Rodriguez J 1993 *Physica* B **192** 55–69
[10] Wagh A S, Singh J P and Poeppel R B 1993 *J. Mater. Sci.* **28** 3589
[11] Wagh A S, Poeppel R B and Singh J P 1991 *J. Mater. Sci.* **26** 3862
[12] Reddy Ravinder R, Prakash O and Venugopal Reddy P 1995 *Appl. Supercond.* **3** 215
[13] Anderson O L 1965 *Physical Acoustics* vol IIIB, ed W P Mason (New York: Academic) p 43
[14] Zhu C and Zheng R 1999 *J. Phys.: Condens. Matter* **11** 8505
[15] Li K, Li X, Liu C, Zhu Z, Du J, Hou D, Nie X, Zhu J and Zhang Y 1997 *Phys. Rev.* B **56** 13662
[16] Zhu C, Zheng R, Su J and He J 1999 *App. Phy. Lett.* **74** 3504
[17] Zainullina R I, Bebenina N G, Ustinova V V and Mukovskii Ya M 2004 *J. Magn. Magn. Mater.* **272** 473
[18] Jahn H A and Teller E 1937 *Proc. R. Soc.* A **161** 220
[19] Chen C X, Qian T, Zheng R K, Wang F and Li X G 2004 *Phys. Status Solidi* b **241** 1827
[20] Chen C X, Zheng R K, Qian T, Liu Y and Li X G 2005 *J. Phys. D: Appl. Phys.* **38** 807–10
[21] Melcher R L 1976 *Physical Acoustics* vol XII ed W P Mason and R N Thurston (New York: Academic) pp 1–77
[22] Melcher R L 1973 *Proc. Ultrasonic Symp. 1973 (IEEE)* pp 293–8